Chapter 4

DATA PROCESSING

The objective of this work, as has been pointed out in the introduction, is to assess the appropriateness and effectiveness of the gravity method in finding the location and defining the structures of a granite cupola buried underneath metamorphosed sediments and volcanic rocks. To achieve this goal, it is necessary to process the collected data as accurately as possible. This chapter presents discussion of the actual reduction processes applied to the gravity measurements.

To reduce the gravity values to a single plane of reference the following corrections were applied:

1. meter-drift correction;

2. latitude correction;

3. free-air correction;

4. Bouguer plate correction, and

5. terrain correction.

A FORTRAN computer program was used to speed up calculations of the corrections applied to the measurements over the stations in the gridded area. The listing of this computer program named MAIN.FOR can be found in the appendix along with examples of the input and output data sets.

Upward continuation (to 200 m) of the gridded data was done after their reduction to a common plane of reference.

The corrections for the stations in the 7-km line were calculated following the same principles and formulas on which the computer program was based using a pocket-sized scientific calculator.

After applying the corrections the 7-km Bouguer anomaly profile was smoothed by finding a polynomial that approximately fits it.

4.1 Meter-drift Correction

In the course of operating the gravity meter, the very sensitive springs inside the instrument are subjected to stress. This causes the springs to be strained and consequently to stretch gradually and continuously as the survey progresses. Coupled with this stress-strain effect are the effects of temperature change and of the changes in the earth's tides. This tidal effect is due to the variations in the pulling force exerted by the sun and the moon on the earth. The effect of the temperature is only substantial when the meter is subjected to extreme and sudden changes in temperature. Most of the modern gravity meters are equipped with temperature-regulating devices and careful acclimation of the meter at the start of each day's survey reduces this effect further. Most of the drift correction applied to the gravity readings or values is made necessary by stress-strain and tidal effects. Any combination of these effects causes the gravity meter readings to drift either upward or downward.

An upward drift occurs when the reading taken at a later time (second reading) over a certain station is higher than a previous reading (first reading) recorded earlier for the same station. When the second reading is lower than the first, a downward drift is said to have occurred. This "drifting" is the main reason for taking at least two readings at two different times over every station for the purpose of monitoring it and computing for its contribution to the gravity readings recorded. The survey procedures which are usually followed in practice to monitor this drift have been described in Chapter 3.

Aside from these drifting effects, the springs inside the gravity meter also creep with time even if it stays in only one place and is not being used. Therefore it is good practice to use only one gravity meter throughout the survey. In doing the gravity surveys over the gridded area, however, the use of two gravity meters was unavoidable. The first meter, manufactured by SCINTREX with an instrument constant of 1.1021 g.u./s.d., was damaged in an accident and had to be sent back to Canada for repairs. The second meter used was also manufactured by the same company and is of the same type as the first one but with a different instrument constant (0.9713 g.u./s.d.). Both meters have a sensitivity of 0.1 g.u.

The first meter, with a post-repair instrument constant of 1.096 g.u./s.d., was used in running the gravity survey over the 7-km traverse line.

4.1.1 Creep and Drift Corrections: Stations in the Gridded Area

The calculation of the drift corrections applied to the stations in the gridded area consisted of two steps. The first step was to calculate the relative differences between the control stations graphically and to correct for any closing errors found. The second step was to compute the drift corrections for the intermediate stations.

First Step. This can be explained more easily with the use of an example such as shown in Figure 4.1 where gravity readings are plotted against the time at which corresponding readings were taken.

In Figure 4.1, suppose M denotes the first and N the second reading at station 11500N 10000E, O and P are first and second readings, respectively, at station 12000N 10000E while IO is the interpolated reading on station 11500N 10000E at the time O was taken at station 12000N 10000E and IN is the interpolated reading on station 12000n 10000E at the time N was taken at station 11500N 10000E.

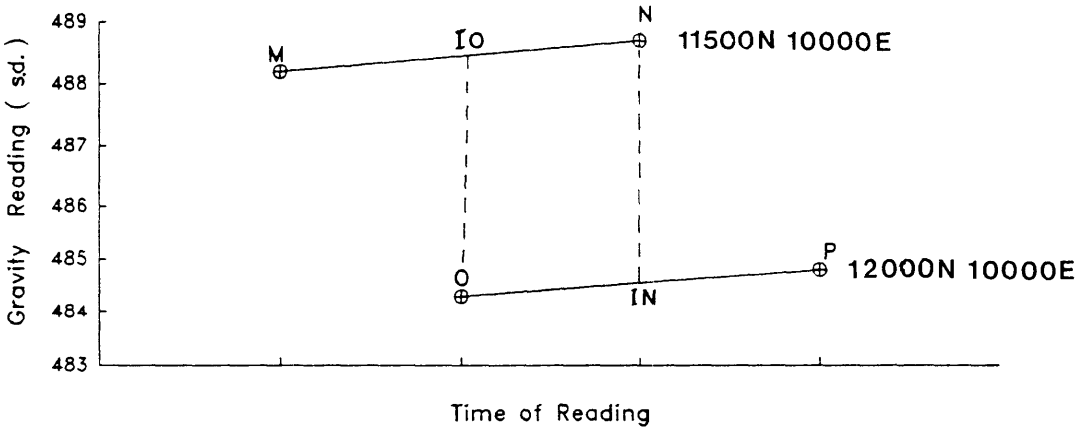

Figure 4.1 An Upward Drift Curve

Assuming that the meter drift is linear and using the values IO = 488.15 s.d., O = 484.20 s.d., N = 488.50 s.d., and IN = 484.25 s.d., the drift correction can be reasonably distributed to the two stations by subtracting O from IO, IN from N and averaging the two differences.

Thus,

$$IO - O = 488.15 - 484.20 = 3.95 \text{ s.d.}$$

and

$$N - IN = 488.20 - 484.25 = 3.95 \text{ s.d.}$$

The average of the two differences just calculated is taken as the difference between the gravity values of the two stations. This difference (in scale divisions)is converted to gravity units by multiplying its value with the meter constant. In this particular example the constant is 0.9713 g.u./s.d.. Thus, the difference is equal to

$$3.95 \text{ s.d. x } 0.9713 \text{ g.u./s.d.} = 3.83 \text{ g.u.}$$

The example used above, though actually acquired, is an ideal case. In most cases the curves are not exactly parallel even though the meter drift is linear; thus the two differences between the interpolated and actual readings are not equal. In cases like these the same procedure described above is nevertheless used to calculate the differences between the gravity values of any two control stations.

The discrepancy just mentioned may be attributed to errors either in reading or setting up the instrument or to a combination of both and some other personal errors. The effects of these errors become more evident and significant when all the " value differences" are plotted as shown in Figure 4.2.

The nodes in Figure 4.2 represent control stations. The arrows point to the station the value of which is higher than that of the station at the tail. The values in the middle of the rectangles are closure errors. Had there been no error in the survey, the sum of the "clockwise differences" would have been equal to that of the "counterclockwise differences" for every loop in Figure 4.2. As it is, misclosures occur: -0.58 g.u. in Loop 1, +0.895 g.u. in Loop 2, +0.385 g.u. in Loop 3, etc., considering the "clockwise differences" as positive and the "counterclockwise differences" as negative.

An algorithm designed by Green (1962) for distributing these errors by least squares was utilized in distributing errors to all the control stations in the gravity survey network.

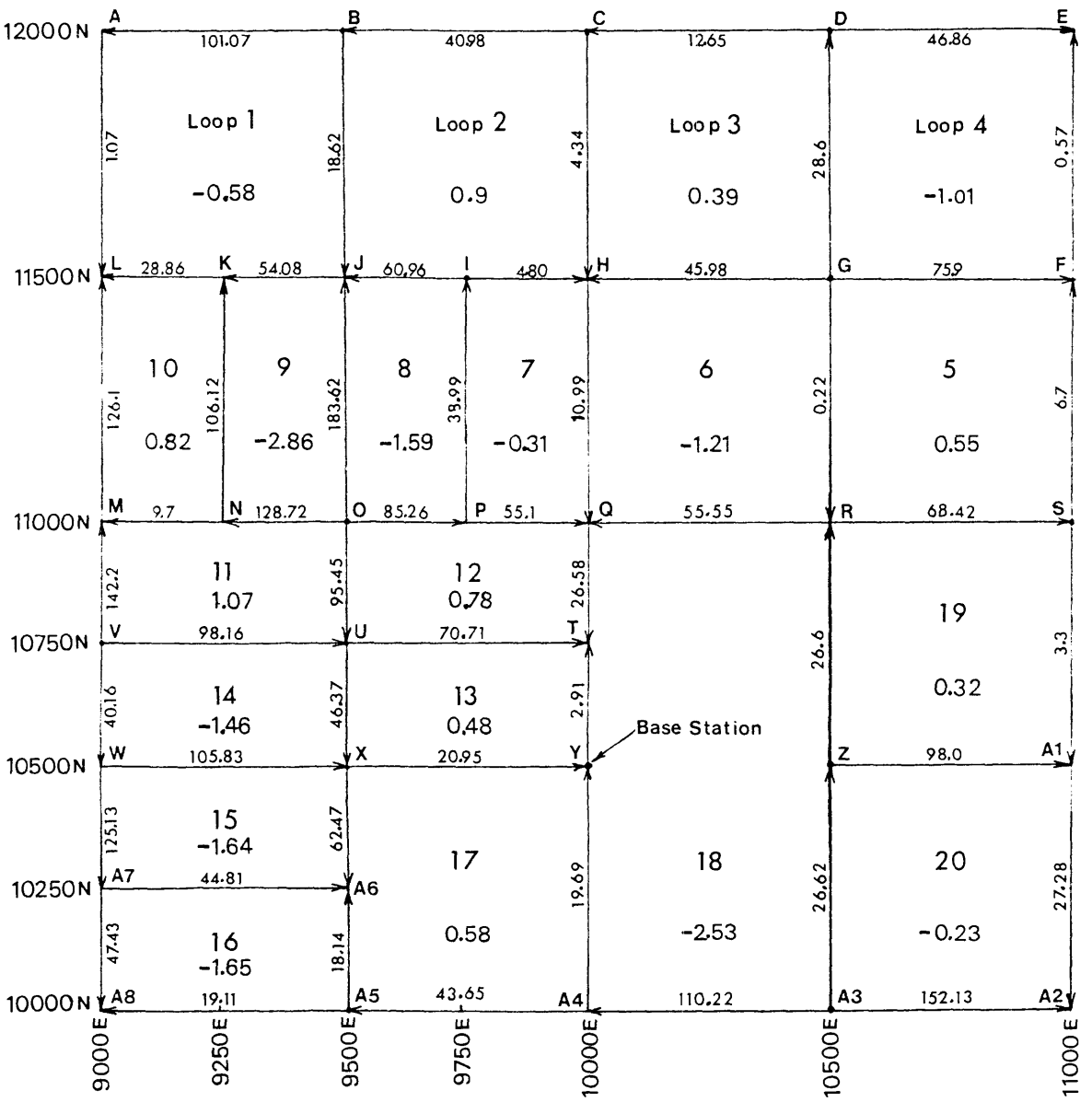

Figure 4.2 The Gravity Survey Network of the Gridded Area.

Second Step. After applying the misclosure adjustments to the differences between control stations, a control table (Table 4.1) was prepared as the next step in calculating the drift corrections to be applied to the intermediate stations.

STATION	G.U.	S.D.
12000N 09100E	670.6	691.34
12000N 09500E	570.1	587.73
12000N 10000E	529.5	† 481.32
		545.87
12000N 10500E	517.2	† 470.14
		533.20
12000N 11000E	564.4	† 513.05
		581.86
11500N 09000E	671.1	691.86
11500N 09250E	642.1	661.96
11500N 09500E	588.8	607.02
11500N 09750E	528.6	544.95
11500N 10000E	533.9	† 485.32
		550.41
11500N 10500E	488.5	† 444.05
		503.61
11500N 11000E	564.2	† 512.87
		581.65
11000N 09000E	544.6	561.45
11000N 09250E	534.9	551.45
11000N 09500E	405.3	417.84
11000N 09750E	490.0	505.16
11000N 10000E	544.9	† 495.32
		561.75
11000N 10500E	489.3	† 444.78
		504.43
11000N 10850E	585.1	† 531.90
		603.19
11000N 11000E	557.7	† 506.96
		574.95
10750N 09000E	402.0	414.44
10750N 09500E	500.6	516.09
10750N 10000E	571.3	† 519.32
		588.97
10500N 09000E	441.4	455.06
10500N 09500E	547.3	564.23
10500N 10000E	568.2	† 516.50
		585.77
10500N 10500E	463.3	† 421.14
		477.63
10500N 11000E	561.3	† 510.23
		578.66
10250N 09000E	565.6	583.10
10250N 09500E	610.2	629.07
10000N 09000E	612.2	631.14
10000N 09500E	592.3	610.62
10000N 10000E	548.2	† 498.32
		565.15
10000N 10500E	437.2	† 397.41
		450.72
10000N 11000E	588.9	† 535.32
		607.11

Table 4.1 Control Table: control values (in s.d.) for stations surveyed using the meter with an instrument constant of 1.1021 g.u./s.d. are highlighted by the symbol †.

Calculation of Values in Table 4.1. The first reading, 516.50 s.d., recorded at the base station, 10500N 10000E, was multiplied by the first meter constant (1.1021 g.u./s.d.) to obtain its value (568.2 g.u.). The value of the next control station, 10500N 9500E, was obtained by subtracting the difference (20.9 g.u.) between its value and that of the base from the value of the base. Subtraction was performed because the readings (hence the value) at this station were lower than those recorded at the base. Had the value of the base been lower, addition would have been performed instead. The control reading for traverses where the first meter was used was calculated by dividing this value (547.3 g.u.) by the meter constant (1.1021 g.u./s.d.). The control reading in cases when the second meter was used was obtained by dividing the same value by the second meter constant (0.9713 g.u./s.d.). This process, in effect, has been used to determine the readings at all control stations that would have been recorded had the readings been taken at the same time as the first reading recorded at the base using either meter. This approach in computing for the drift correction, together with the use of two meters, is seldom encountered and deserves further explanation.

In Figure 4.3 the letter A represents the very first reading recorded on the base station and B the reading on another control station that would have been read on it at the time A was recorded at the base station. In Figure 4.3, the point B is plotted to have been read at a time different to when A was read because this represents the actual field situation. Because of the slow-creep phenomenon in all spring systems, the reading at any control station will change in time even if the meter is not moved. For this reason, the readings in the base were not the same when it was used as a control station for the detailed traverses. C represents this later reading. The difference between A and C is equal to the difference between B and D if no additional drift occurs during a detailed traverse. This did happen at times when the survey traverses were completed in relatively shorter time. However,this was not usually the case. Either an updrift or a downdrift occurred. The usual procedure to monitor these smaller drifts is to use only one control station as the point of reference, i.e., after readings at the intermediate stations the meter is taken back to the starting station. The drift is the difference between the readings taken at that station. As has been mentioned previously in Chapter 3, the survey was completed in a shorter time by maximizing the use of all the control stations. Instead of a final reading at the starting control station, the detailed traverses ended with a reading at another control station. In the following discussion it will be explained how to correct for the creep effect and how to calculate the drift corrections for the detailed survey stations.

As has been explained before, the readings in Table 4.1 are readings which should have been recorded at corresponding control station at the time that the first reading on the base was taken and recorded. If a solution can be found to reduce all the readings taken and recorded at the intermediate stations to the same point of reference and time, then the correction for creep can be calculated.

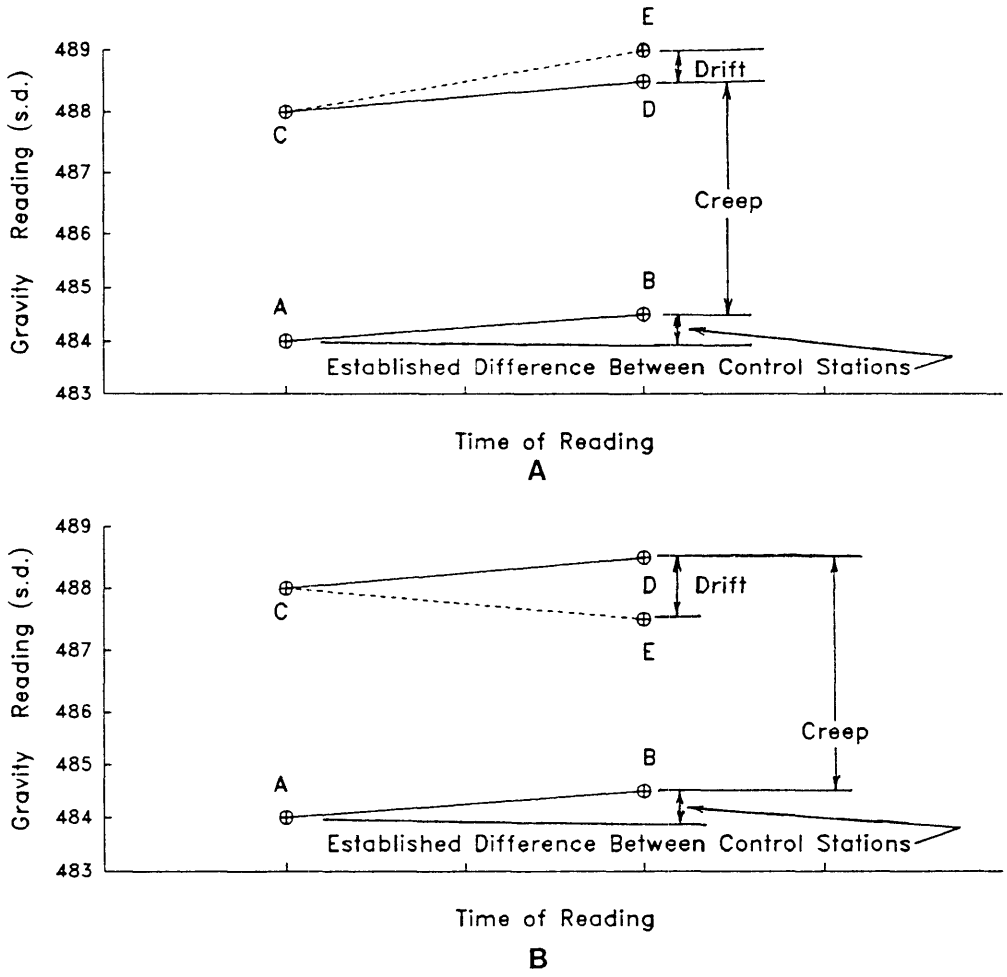

Figure 4.3 Curves and Values Involved in the Calculation of Creep and Detailed Survey Traverse Drift in Case of (A) an Updrift and (B) a Downdrift

A solution is herein proposed and has actually been used in calculating the creep correction for all the intermediate stations surveyed. The amount of meter creep for any control station is the difference between A and C (see Figure 4.3). By subtracting this creep value from readings taken over the intermediate stations, these readings are reduced to a single point of reference (spatial and temporal). If the control readings (in s.d.) are used instead of the values (in g.u.), the use of two meters ceases to matter.

To find the degree of drift that has occurred during a detailed traverse survey the difference between the readings at the two control stations is calculated. This difference is then compared with the previously established difference between the control stations. If the former is higher than the latter then an updrift has occurred. If lower, then a downdrift has occurred. In cases of updrift, the drift correction is subtracted from the observed values of the stations. In cases of downdrift, addition is performed instead. The drift correction is calculated by dividing the degree of drift by the length of time within which it occurred. This process will be clarified further by explaining the computer program routine written to compute both the creep and drift corrections.

From Figure 4.3A E is the reading recorded at the second control station. The value BE is equal to BD + DE (creep + drift) = AC + DE in the case of an updrift. In cases of a downdrift BE is less than BD (see Figure 4.3B). This is the relationship which makes it possible to monitor and compute the value of the drift when two control stations are used.

It has been previously explained why the values in the control table are necessary. Their actual use in computing the drift correction will be described next.

The subroutine DRIFT in the computer program calculates the drift correction applied to the intermediate stations. The values in Table 4.1 were used in the preparation of the input file for the computer program MAIN.FOR. The variable named CONRDG contains the value from the control table for each control station. The variable named SSRDG contains the reading recorded at that control station during the time the station was used as a reference point for a detailed traverse survey. The difference between these two values is computed by the subroutine DRIFT and stored in variable CONDIF which is added to every RIS - reading taken over intermediate stations. This addition has the effect of adjusting the readings at all intermediate stations covered by a traverse to common points of reference in space (base station) and time (time of first reading recorded at the base station). The other variables which are part of the input file and necessary for the computation of the drift correction are RDGB and RDGS, the higher and lower control station reading, respectively, and TDIF - the time interval between the time of reading the starting control station and an intermediate station.

4.1.2 Drift Correction: Stations Along the 7-km Line

The calculation of the correction due to drift for the stations in the 7-km traverse line was simpler. By simple determination of the relative differences between the stations using the same graphical method employed for the control stations in the gridded area, drift corrections were applied.

4.2 Latitude Correction

Latitude correction is applied to observed gravity values or differences because gravity increases from equator to pole. This increase is due to factors and forces that will be discussed below.

It is an established fact that the design and application of gravity meters are based on Newton's law of universal gravitation. This law states that every particle of matter exerts a force of attraction on every other particle that is proportional to the product of the masses and inversely proportional to the square of the distance between them: i.e.,

$$F = G\frac{m_1 m_2}{r^2}$$

where F = the force between two masses, m_1 and m_2, r = the distance between the masses and G = the universal gravitational constant = 6.67 x 10^{-11}Nm^2 kg^{-2}.

It has also been established that the earth is not a perfect sphere. The best approximation for the shape of the earth for practical purposes is an ellipsoid of revolution for which a balance is maintained between the gravitational forces tending to make it spherical and the centrifugal forces of rotation tending to flatten it (Nettleton, 1976). As a result of this balance the equatorial radius is about 21 km greater than the polar radius. This is known as the reference ellipsoid and is virtually the sea-level surface. Any point on the pole is therefore nearer to the centre of the earth than any point on the equator. According to Newton's second law of motion expressed mathematically as $F = ma$, the force exerted on a mass is directly proportional to its acceleration. Both F and a are therefore inversely proportional to distance. It follows then that the acceleration of gravity should be greater at the poles than at the equator. The increase in gravity due to this distance factor has been determined to be approximately 6.63 x 10^4 g.u. (Hammer, 1943).

As has been mentioned above, other factors and forces contribute to the difference between the polar and equatorial gravitational acceleration. The outward centrifugal acceleration at the equator, which is absent at the poles, contributes an increase of 3.39 x 10^4 g.u. Because of the mass-shape factor, the attraction of the whole earth is greater at the equator than at the poles making a decrease of 4.85 x 10^4 g.u. (Hammer,1943). The sum of these effects is 5.17 x 10^4 g.u.

The variation of gravity with latitude over the surface of an ellipsoid earth can be expressed in the form

$$g = g_o \ (\ 1 + C_1 sin^2\phi - C_2 sin^2 2\phi)$$

where g_o is the value of gravity on the equator and ϕ is the latitude. C_1 and C_2 are constants which depend on the earth's shape the numerical values of which have been adjusted to give a best fit to the measured variation of gravity over the earth's surface (Griffiths and King, 1983).

The shape of the earth is expressed in terms of the dimensions of an ideal spheroid of reference. The dimensions usually given are the equatorial and polar radii a and b, respectively, or the equatorial radius together with the flattening; i.e.,

$$f = \frac{a - b}{a}$$

Several slightly different spheroids and corresponding gravity formulas have been determined from time to time as the amount and precision of gravity and geodetic information have increased. Those that are useful with regard to the reduction of gravity readings in geophysical prospecting are commonly used in making corrections for the normal northward or southward gravity increase (Nettleton, 1976). Those formulas were not used by the writer and therefore will not be discussed here.

Parasnis (1973) formulated working equations which are easier to use for calculating latitude corrections when the distance between the base and a station is known in relative gravity surveys.

For distances which are less than 2 km, the latitude correction may be calculated easily by using the formula

$$\Delta g_{\phi} = 0.081 \ sin2\phi \ \text{g.u. per 10 m N} - \text{S distance} \qquad (4.1)$$

where ϕ is the latitude of the base. If the station is on a higher latitude (that is north of the base if both are in the northern hemisphere and south of it if they are in the southern hemisphere) the latitude correction must be subtracted from the observed value. In the opposite case it must be added to it.

For distances greater than 2 km on either side of the base, the gravity difference from the base is not strictly proportional to the distance within the accuracy required (Parasnis, 1973). The exact correction in this case may be computed using Parasnis's formula below,

$$\Delta g_{\phi} = 51723 \ (sin^2\phi_1 - sin^2\phi_0) \ \text{g.u.} \qquad (4.2)$$

where ϕ_1 and ϕ_0 are the latitudes of the stations and the base, respectively.

For the latitude correction to be accurate within 0.1 g.u. - an accuracy which must be aimed at in ore prospecting - it is sufficient that the north-south distance between the base and the station be known to within 10 metres (Parasnis, 1973).

4.2.1 Latitude Correction: Stations in the Gridded Area

The subroutine LATUDE of the computer program was based on Parasnis's formula (Equation 4.1). The subroutine is called after the values corrected for drift have been returned from subroutine DRIFT to the main program.

4.2.2 Latitude Correction: Stations Along the 7-km Line

Most of the distances between the base and the stations exceed 2 km. The second formula of Parasnis (Equation 4.2) was therefore used in calculating the latitude correction in this case.

The stations along the traverse line were laid out using the Magnetic North as reference. To reduce the latitudes of the stations with the True North as the reference the following formula was used.

$$\phi_1 = 29.44^0 + N \cos 11.46^0 \text{ x } \frac{1\text{min}}{37\text{mm}} \text{ x } \frac{1^0}{60\text{min}} \tag{4.3}$$

In Equation 4.3 ϕ_1 is the latitude of station in degrees, N is the distance of station from the base (in mm) measured along the traverse line on a 1:50000 topographic map, $37mm$ is the length of 1 minute latitude on the topographic map, 29.44^0 is the latitude of the base station, and $11.46^0 = 10.7^0 + 0.6^0 + 0.16^0$ = the angle between the True North and the Magnetic North (see Figure 4.4).

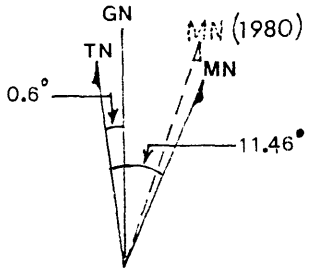

Figure 4.4

Figure 4.4 above is a reproduction of the diagram in the topographic map No. 9239 II & III prepared by the Central Mapping Authority of New South Wales, wherein the True North (TN), Grid North (GN), and Magnetic North (MN) are shown diagrammatically for the centre of the map. Magnetic North is correct for 1980 and moves east by 0.1^0 in approximately 3 years. Since the gravity survey was done during the last quarter of 1985, a value of 0.16^0 was added to the difference between True North and Magnetic North.

4.3 Free-air Correction

As has been pointed out earlier, gravitational acceleration is inversely proportional to the distance separating two masses. Gravity therefore varies with elevation since a point at a higher elevation is farther away from the centre of the earth and therefore has a lower gravitational acceleration than one at a lower elevation. Since gravity varies with elevation, it is necessary to correct all observations to a datum which is usually but not always the sea level. The rate of this normal vertical variation, or the vertical gradient of gravity, can be calculated quite accurately from the gravity formula and the radius of the earth (Nettleton, 1976).

The gravity at a point on the surface of a spherical earth is

$$g = \frac{GM}{R^2}$$

where M is the total mass of the earth and R its radius. The vertical gradient is

$$\frac{dg}{dz} = \frac{dg}{dR} = -\frac{2GM}{R^3} = -\frac{2g}{R}$$

Taking the mean radius of the earth R = 6.367 x 10^8 cm and the theoretical value of gravity at sea level and at 45^0 latitude, g = 980.629 gals, then

$$\begin{aligned} \frac{dg}{dz} &= -\frac{2 \text{ x } 980.629}{6.367 \text{ x } 10^8} \\ &= -3.086 \text{ g.u./m} \end{aligned} \tag{4.4}$$

There is a small second-order term which is appreciable only at high elevations (Nettleton, 1976). Heiskanen and Vening Meinesz (1958) calculated that this term amounts to only 0.7 g.u. for an elevation of 1 km, 3 g.u. for 2 km and 17 g.u. for 5 km or about $0.7h^2$ g.u., where h is in km.

In computing the free-air correction in both the gridded area and the 7-km traverse line, this second term was not included because no elevation difference was greater than 150 metres. The elevation of the base in the gridded area was assumed at 946.32 m while the base for the 7-km line was assigned an elevation of 890.00 m. The free-air correction was added to the observed gravity values of stations higher than the base and subtracted from those of stations lower than the base.

The subroutine FREAIR in the program MAIN.FOR computes this correction for the stations in the gridded area. The subroutine is based on Equation 4.4.

4.4 Bouguer Plate Correction

The free-air correction takes account only of the fact that the station and the base are not at the same distance from the centre of the earth. The rock material between the level of the station and the base, however, exerts an extra gravitational attraction at a station situated higher than the base and therefore tends to increase the gravity difference between them.

Assuming that the rock material is an infinite horizontal slab and of thickness h equal to the difference in elevation between a station and the base, the gravity attraction g for a point on the surface of a slab of thickness h and density ρ is given by Equation 4.5 (Parasnis, 1979)

$$\begin{aligned} g &= 2\pi G\rho h \\ &= 0.4191 \ \rho \ h \ \text{g.u./m} \end{aligned} \tag{4.5}$$

If a station is higher than the base, its gravity value is increased because of the contribution of the slab of material between it and the reference level. If the station is lower than the reference elevation, its gravity value is decreased because of the absence of material between it and the reference level. This correction must therefore be subtracted from the observed gravity value if the station is above the level of the base and added if it is below. The Bouguer plate correction is always opposite in sign to the free-air correction.

4.4.1 Density Determination by Density Profile

The choice of density for the Bouguer plate and terrain corrections for a survey in a new area is often a troublesome problem. It has been one of the problems in this research because the different rock formations in the area surveyed have different densities as determined by laboratory measurements. Experts recommend the use of the density profile method in cases like this.

The density profile consists of a line of stations at close spacing over a topographic feature such as a hill. The measurements are reduced using a range of density values to find the one which minimizes the correlation of gravity with topography. The corresponding density is an average value for the topographic feature sampled (Nettleton, 1976).

The 7-km line transected two hills. The measurements made over these hills were used for computing and plotting the density profiles in Figures 4.5A and 4.5B. The densities used for the computations range from 1.9 to 3.5 g/cc taken at 0.2 g/cc intervals. A density of 2.7 g/cc was considered the appropriate value and was consequently used in calculating the elevation corrections.

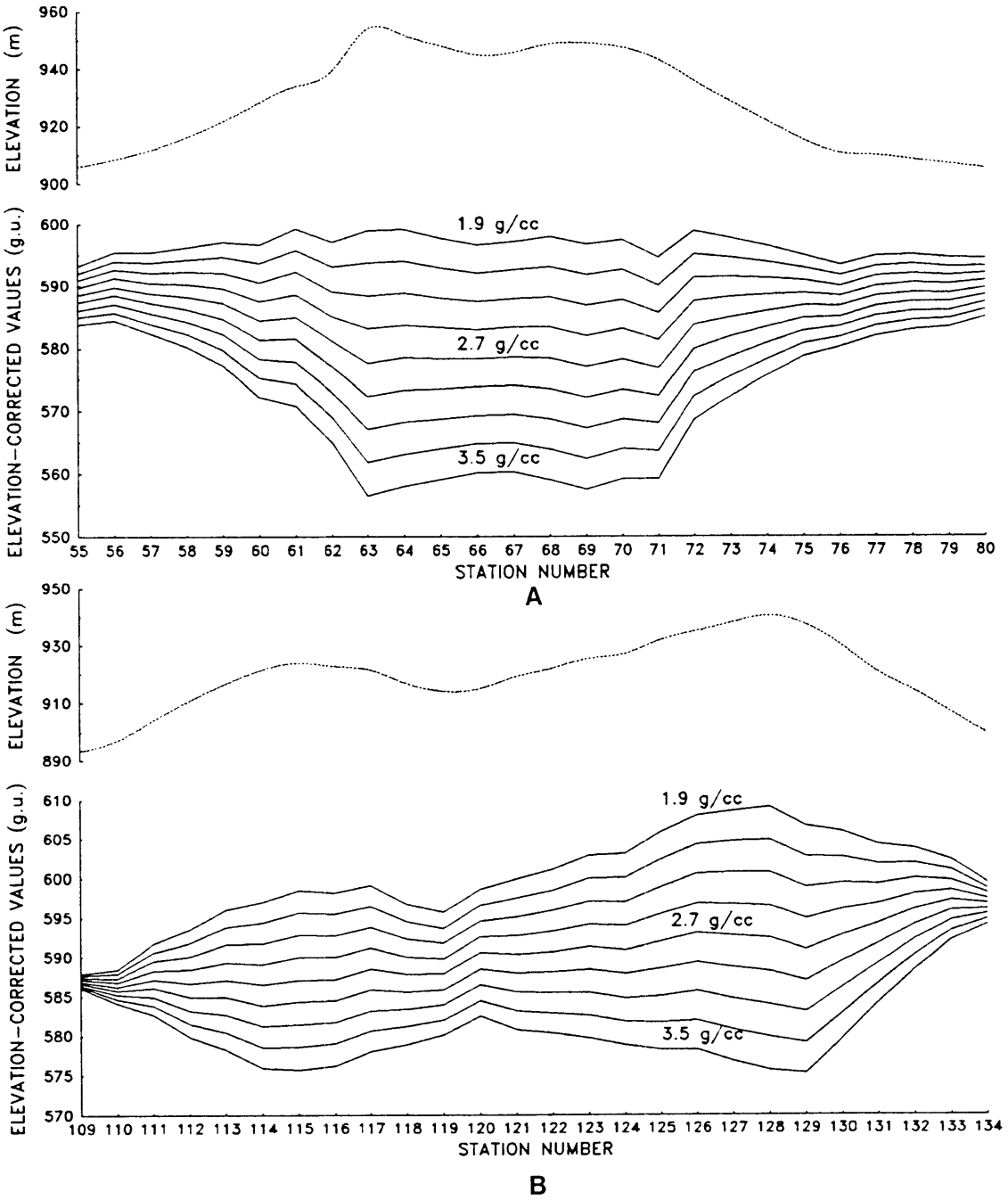

Figure 4.5 Elevation and Density Profiles of the Two Transected Hills.

4.5 Terrain Correction

When the topography is relatively flat, the combined free-air and Bouguer plate correction may sufficiently reduce the data to the reference datum. If there are considerable irregularities of elevation, particularly in the vicinity of the station, then the single assumption that there is an infinite slab of rock between the station and the reference datum is, however, inadequate and a further allowance is needed for departures from this.

Hammer (1939) showed the importance of terrain correction by using an actual gravity profile across Sierra Madera, Pecos County, Texas. Without the terrain correction, a negative anomaly was recorded across a mountain but after applying terrain correction, a positive anomaly was obtained instead. Since then, Hammer's method and table have been considered more or less the standard in calculating the terrain correction specifically in gravity prospecting work. Hammer's method can be summarized as follows.

The area around the station is divided into zones and compartments, for example, by laying a transparent terrain-correction zone chart upon a topographic map and centring it at the gravity station. The average departure without regard to sign of the topography in each compartment from the plane through the station is then determined and the terrain correction corresponding to this average departure is evaluated for each compartment by means of tables calculated for that purpose. Finally, these terrain corrections are summed over all the zones in which there are appreciable effects and the sum multiplied by a factor for the density to obtain the total terrain correction for the station.

The calculation of Hammer's tables is based upon the formula (Equation 4.6) for the gravitational attraction of a vertical hollow cylinder at a point on the axis and in the plane of one end of the cylinder.

$$g = 2\pi G\rho \left[R_2 - R_1 + \sqrt{R_1^2 + h^2} - \sqrt{R_2^2 + h^2} \right] \tag{4.6}$$

In Equation 4.6 R_1 and R_2 are the inner and outer radii, h is the height of the cylinder (representing the average height of the terrain), G is the universal gravitational constant and ρ is the density of the surface rocks. The calculations were

carried out by solving this equation for h in terms of the radii and an adopted unit gravitational attraction for one compartment.

Hammer (1939) considered the contribution of the area within two metres of the station to the terrain correction as negligible. He nevertheless proposed a formula for calculating the terrain effect of this small area for very extreme terrain conditions such as when a station is on a hillside. The terrain effect within a circle of radius R of a plane inclined at an angle θ from the horizontal and passing through the gravity station is given by

$$T_R = 2G\rho R\ [\pi - 2\cos\theta \bar{K}(\sin\theta)]\ \text{x}\ 10^4 \tag{4.7}$$

where T_R is the total terrain correction in g.u. for an inclined plane out to a distance of radius R in cm from the station (Figure 4.6), G is the universal cgs gravitational constant, θ is the slope angle, ρ is the density expressed in g/cc, and $\bar{K}$ is the complete elliptic integral of the first kind (Hammer, 1939).

Sandberg (1958) used Equation 4.7 in calculating the terrain effects of familiar land forms such as valleys, ridges and hillsides and prepared a table which can be used to approximate more easily and quickly the terrain effect of these land forms. The values in Sandberg's table are in the same denominations and are interchangeable with the Hammer chart and table zone for zone. Sandberg's table can therefore be used in combination with Hammer's chart and table.

The two methods discussed above were used in calculating the terrain corrections for the stations in the gridded area. Sandberg's table was utilized for areas wherein features could be approximated as either a hillside, a ridge or a valley, while Hammer's were used for areas farther away from a station. The sum of all the effects of all compartments was made part of the input file for the computer program. The total terrain correction for each station was computed by the subroutine TERAIN. The results obtained indicated that the combined effects of the small hills and valleys within and farther away from the survey area were not large enough to change the gravity values significantly. For this reason, the terrain corrections for the 7-km line stations were calculated using Sandberg's method only.

4.6 Upward Continuation: Gridded Area

A computer program written by Balia (1981) was utilized in calculating the values at 200 m above the datum level of the survey over the gridded area. Balia's program was, however, modified first by replacing the original weighting coefficients with those calculated by Peters (1949). Although Peters's coefficients were originally used in the interpretation of magnetic data, they can be utilized in gravity data because the two are both potential field data.

4.7 Polynomial Fit for the 7-km Gravity Profile

The observed profile (Figure 4.6) obtained after the reduction discussed above apparently still contains "noise". These unwanted components may be attributed either to observational errors, insufficient terrain corrections, effects of near-surface lithological variations or any combination of the three. Several smoothing or filtering operations are available to smooth out these unwanted components. Polynomial fitting is one of the simplest to use and was consequently employed in smoothing the observed profile. A polynomial of the 7th degree (Figure 4.6) gave a satisfactory approximate fit to the corrected profile.

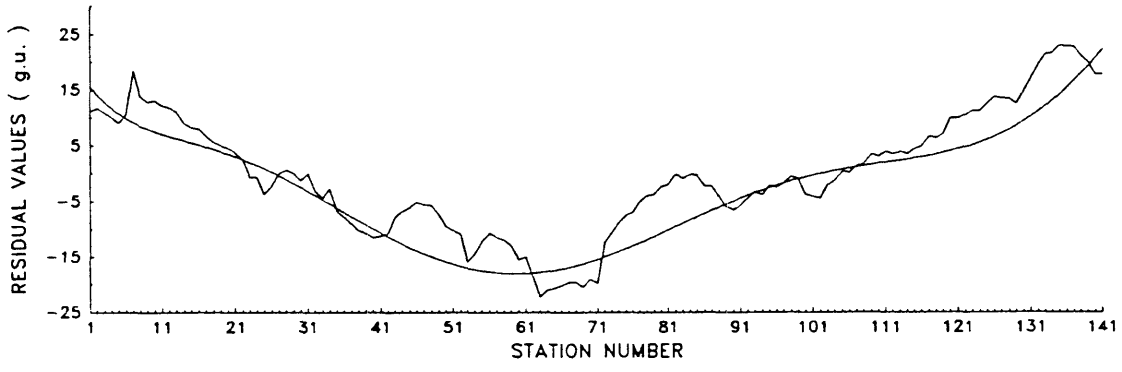

Figure 4.6 The 7-km Observed Gravity Profile and the 7th degree Polynomial.

Chapter 5

INTERPRETATION OF RESULTS

5.1 Qualitative and Semi-quantitative Interpretations: Gridded Area

Only qualitative and semi-quantitative interpretations of the Bouguer anomaly map (Figure 5.1) were made because additional information such as drillhole data which could aid in quantitative interpretation was not available for the study area.

Figure 5.1 Bouguer Anomaly Map of the Gridded Area: Gravity values are relative to the base station, 10500N 10000E; Contour interval = 5 g.u.

In Figure 5.1 the colours represent corresponding ranges of gravity values: blue - 540 to 550 g.u., orange - 550 to 560 g.u., green - 560 to 570 g.u., red - 570 to 580 g.u., violet - 580 to 590 g.u. and black - values greater than 590 g.u.

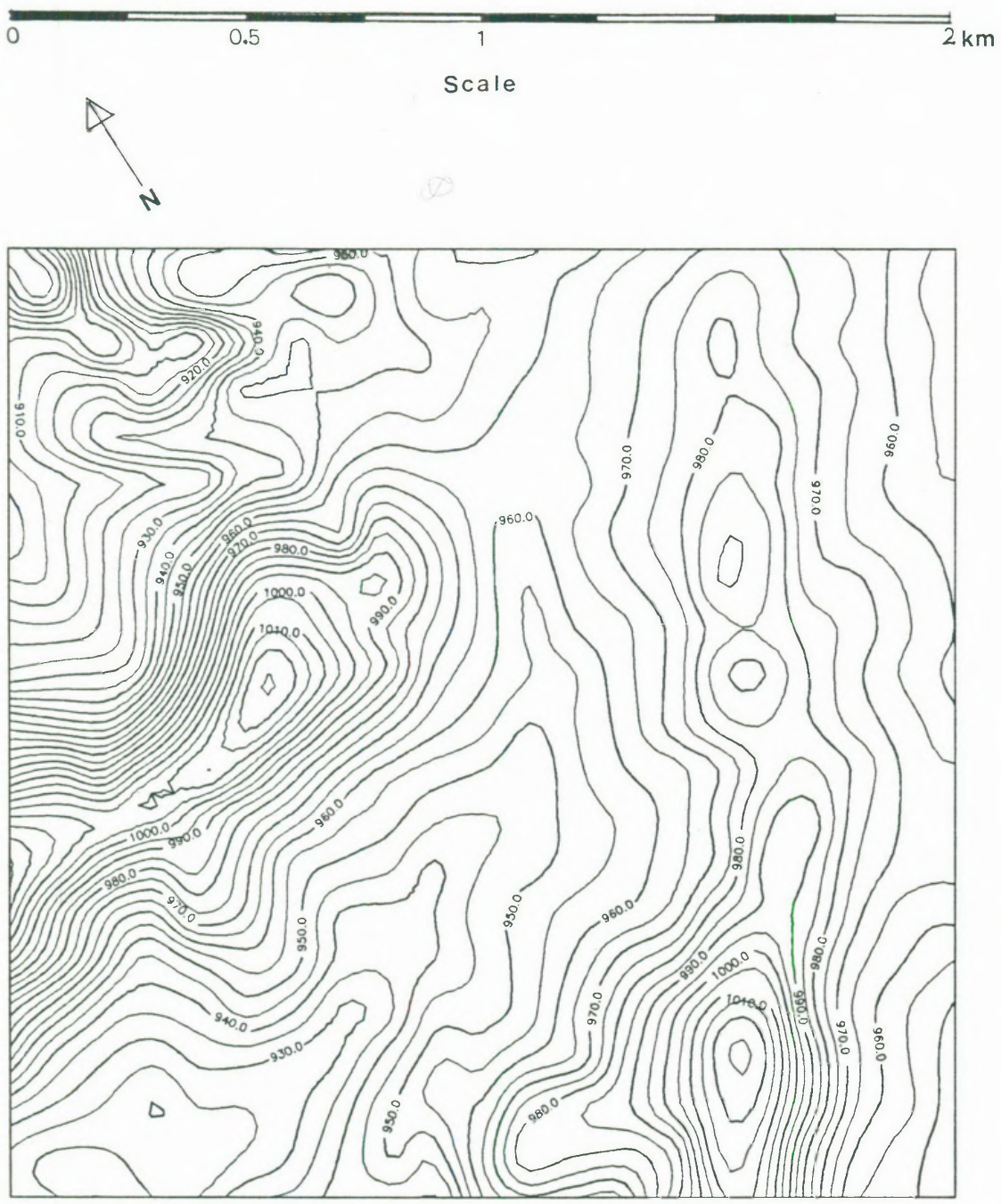

Figure 5.2 Topographic Map of the Gridded Area: Reproduction of the topographic map prepared by EZ-Loloma Joint Venture; Contour interval = 5 m.

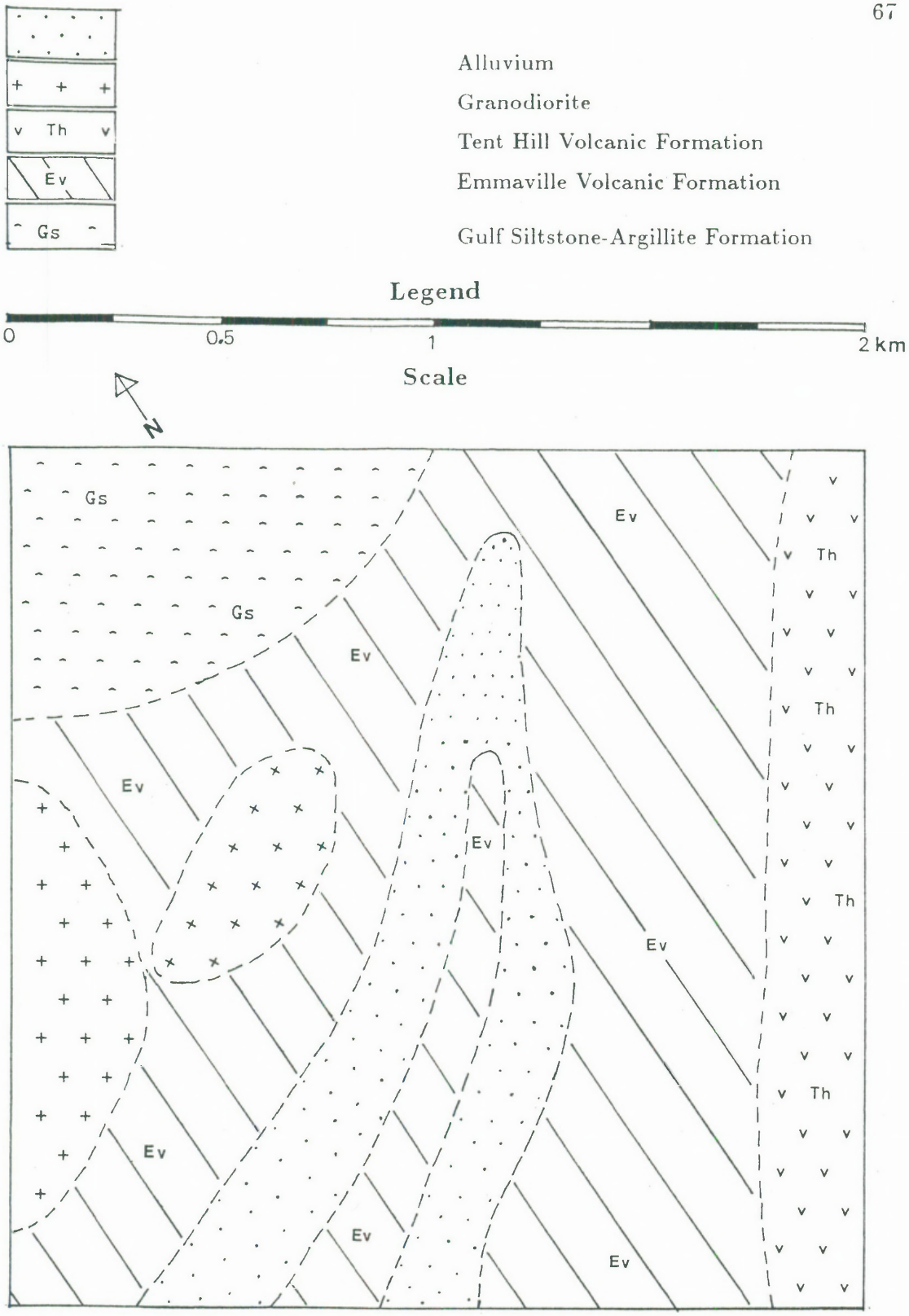

Figure 5.3 Geological Map of the Gridded Area. Additional geological mapping was done by the author in the field leading to some inconsistencies between this map and that shown in Figure 2.3.

The Bouguer gravity anomaly map (Figure 5.1) is characterized by a broad band stretching in an approximately E-W direction with fairly constant gravity values (570 g.u.). Gravity values increase by 10 to 20 g.u. towards the northwestern and southeastern part of the map. It is not clear whether this anomaly pattern is caused by subsurface mass distribution. Superimposition of the gravity map (Figure 5.1) on the topographic map (Figure 5.2) shows that over the area of low topographic relief Bouguer anomalies also exhibit small variations. In the northwestern and southeastern parts the terrain is more rugged and gravity anomalies are higher than in the central part of the study area. After correlation of the gravity map with the geological map (Figure 5.3) the low gravity values have been observed to correspond mainly with alluvial sediments, the minor intrusives and the Emmaville volcanics. The trend of the isogals in the southeastern part clearly follows that of the contact between the Tent Hill Volcanic Formation and the Emmaville Volcanic Formation.

The presence of several rock varieties with different densities within the Emmaville Volcanic Formation contributes to the problem of resolving the bodies causing the small anomalies. Considering that the method by which the elevations used in calculating the elevation corrections were obtained was not as accurate as usually required, these small anomalies may be suspected to have been caused by topographic effects.

Upward continuation of the Bouguer anomaly map was performed to find out if any trend caused by deep structures such as a granite rise or shelf could be discerned. The trend of the isogals (see Figure 5.4) indicates that such a structure may exist underneath the area. This trend, however, can also be attributed to a thick slab of the Emmaville Volcanic Formation which is of lower density relative to the other two bounding formations. A semi-quantitative interpretation of an upward-continuation anomaly profile was made using the Bouguer plate correction formula (Equation 5.1) given by Parasnis (1979).

$$\Delta g = 0.4191\ \rho\ h \text{ g.u./m} \qquad (5.1)$$

In Equation 5.1 ρ is the density contrast and h is the thickness of the Bouguer slab. The thickness of the Emmaville Volcanic Formation was calculated to be approximately 500 metres as shown in Figure 5.5. The dips in the boundaries between Gs, Ev an Th (Figure 5.5B) are not based on observational data. They are assumed and thus have been drawn as dashed lines. The author is of the opinion that the assumption about the dips is not critical for the purpose of the semi-quantitative interpretation where the emphasis is on the depth of the causative body.

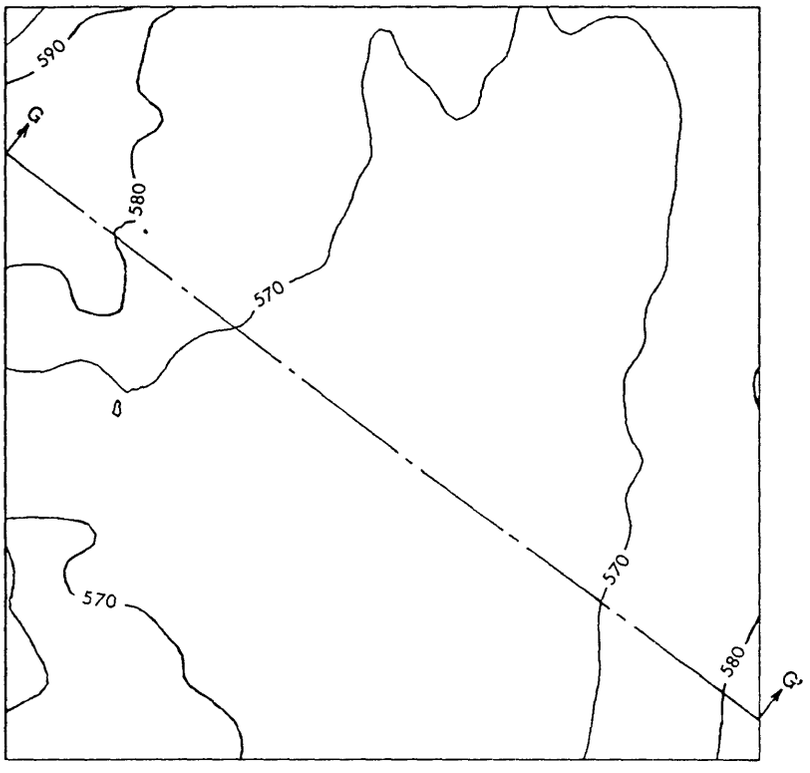

Figure 5.4. Upward-continuation Gravity Map of the Gridded Area

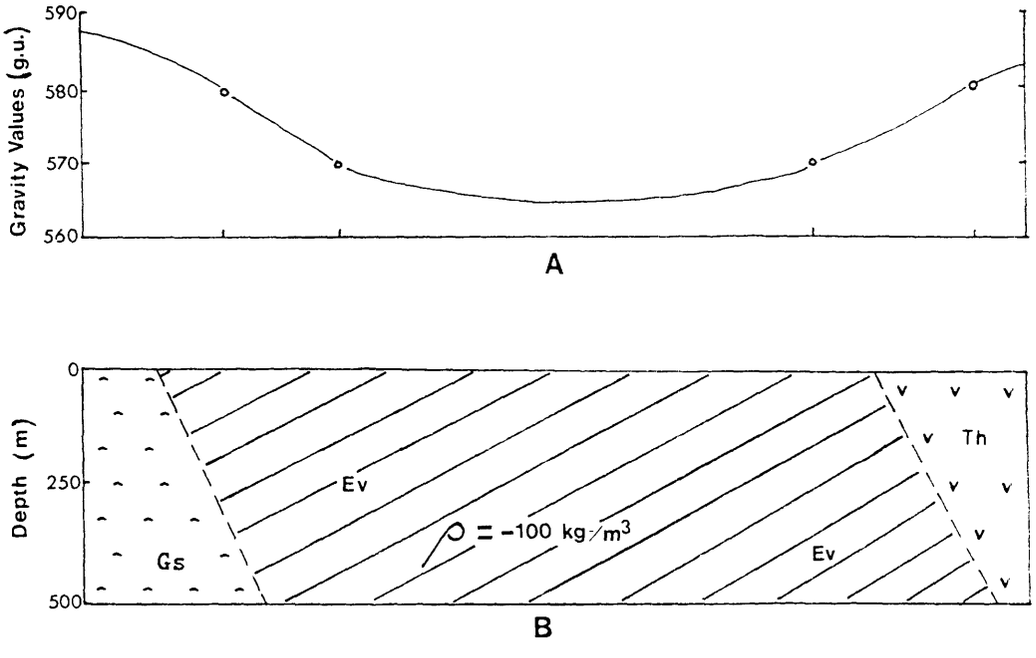

Figure 5.5 (A) Bouguer Anomaly Profile (G-G') from the Upward-continuation Gravity Map of the Gridded Area (B) Simple Geological Model for the Broad Minimum in the Profile G-G'

5.2 Quantitative Interpretation: 7-km Gravity Profile

Two well-known and commonly used methods of interpretation were employed in finding the geological model that would reasonably account for the long-wavelength low-amplitude anomaly detected by the gravity survey run along the 7-km traverse line. The first, spectral analysis, was used in determining initial estimates of the parameters (depth to the top and bottom of the body) of a granite model. It was also used in assessing the amount of geological information actually captured in the survey data. The second method, a gravity modelling technique, usually referred to as Talwani's method, was utilized in finding the models that give reasonably good fit to the observed profile. Available geological information and actually measured rock densities of the survey area were later used in a process of elimination to determine the most plausible geological model.

5.2.1 Spectral Analysis

The spectral analysis of gravity data has long been recognized by geophysicists as a useful tool in gravity interpretation. Odegard and Berg (1965) carried out frequency analyses of gravitational fields of several bodies of simple geometric shapes such as the cylinder, sphere, single fault with a vertical edge, and showed that the depth and size of the causative body may be obtained from the frequency spectrum of the anomaly. Bhimasankaram *et al.* (1977) and Rao and Avasthi (1973) have used a similar approach in analyzing the gravity effect of two-dimensional trapezoidal prisms and that of a two-dimensional triangular prism, respectively.

Initial Estimates of Model Parameters. Hasegawa (1978) has derived mathematical expressions amenable to high-speed digital computing for doing numerical Fourier transformation and has applied his algorithm with a certain degree of success in interpreting the gravity data of the island of Java, Indonesia. Hasegawa's algorithm is very similar to that of Cianciara and Marcak (1976) who have proposed an approach of interpreting gravity anomalies by means of local power spectra. They introduced a statistical model of the medium as source of a gravimetric anomaly. With this model the parameters of the medium are estimated on the basis of the statistically transformed power spectrum of the gravity anomaly.

Figure 5.6 is a plot of the power spectrum of the 7-km gravity profile obtained by employing Hasegawa's technique. Two depth envelopes can be discerned by drawing straight lines through the points. Since the gradients of these two lines are defined by the depths to the upper surface of the body (Johnson *et al.*, 1977), the depths to the two gravity horizons can be calculated using the following formula given by Hasegawa (1978).

$$d = -0.25 \frac{ln\ E1 - ln\ E2}{r_1 - r_2} \tag{5.2}$$

In Equation 5.2 $E1$ and $E2$ are spectrum amplitudes and r_1 and r_2 are the corresponding frequencies.

The depths to the two gravity horizons have been calculated to be 0.35 km and 1.1 km respectively. These two values were used as initial estimates for the depth to the top and bottom of a granite model (Figure 5.7A).

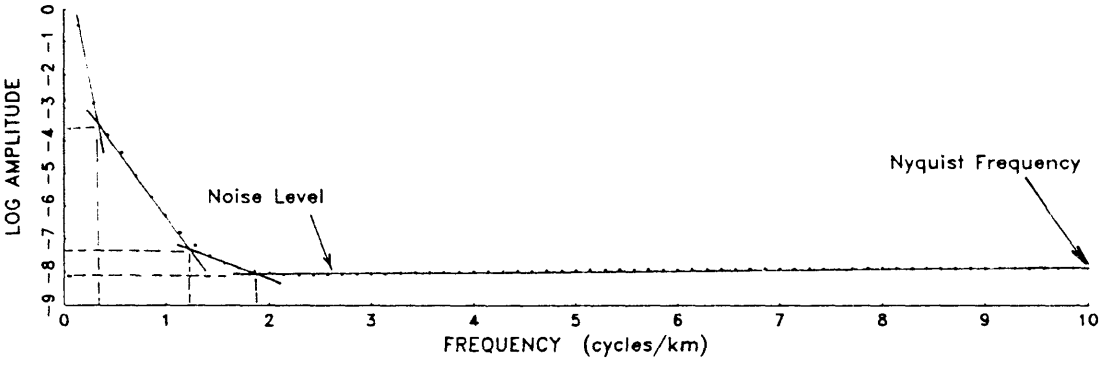

Figure 5.6 Power Spectrum of the 7-km Gravity Profile

Amount of Information in the Data. Johnson *et al.* (1977) have suggested that the information actually captured by a survey can be assessed (*ex post facto*) as follows. A Fourier transform of the data is calculated and the logarithm of the amplitudes is plotted against frequency. Any gravity field will plot below a depth envelope - a straight line whose gradient is defined by the depth to the upper surface of the body. At high frequencies the amplitudes should be approximately equal, indicating that the noise level of the data has been reached. The amount of information in the data can be estimated by the ratio between the frequency at which the noise level is reached and the maximum (Nyquist) frequency. Hence the effective number of data values is given by the original number of data values reduced by this ratio.

In Figure 5.6 it is shown that the noise level has been reached at a frequency of 2 cycles/km. The ratio between this frequency and the Nyquist frequency (10 cycles/km) is equal to 0.20. The effective number of data values is therefore equal to 28 (140 x 0.2). Thus the amount of information in the data would be one fifth of the total number of data values.

5.2.2 Modelling by Talwani's Method

Talwani, Worzel and Landisman (1959) derived mathematical expressions for the vertical and horizontal components of the gravitational attraction due to a two-dimensional body of arbitrary shape by approximating it to an n-sided polygon. The expressions are in forms suitable for solution by high-speed digital computers. Lawton (1978) has written a computer program in FORTRAN based on Talwani's algorithm. This computer program was utilized in finding the geological model that fits the long-wavelength low-amplitude anomaly.

Two models were investigated and both gave satisfactory fit to the observed gravity profile. The first, herein referred to as the granite model, is an approximation to a low-density granitic intrusion into the Emmaville volcanics. The second, referred to as the "basin" model, assumes a basin-like structure of low-density rocks overlying the denser Emmaville volcanics. The fact that two models can be constructed which are consistent with the observations is not surprising, as a unique solution for the inverse problem in gravity interpretation does not exist (Parasnis, 1962).

As has been mentioned earlier, the parameters (depths to the top and bottom of the body) estimated by spectral analysis were used as starting values in modelling by Talwani's method. The first granite model tried generated a profile (Figure 5.7A1) which gave a good match to the middle part of the observed profile. Adjustments were made to the parameters of the body until a better fit was obtained (Figures 5.7A2 and 5.7A3). The depths to both the top and bottom of the trapezoidal body (top width = 50 m) were both decreased by 50 metres at a time while maintaining the total mass constant in all the granite models. All the computed profiles generated by the three granite models evidently fall off at the sides and do not match the observed profile very well. It is known that the contribution of a subsurface structure to a gravity anomaly is most significant at

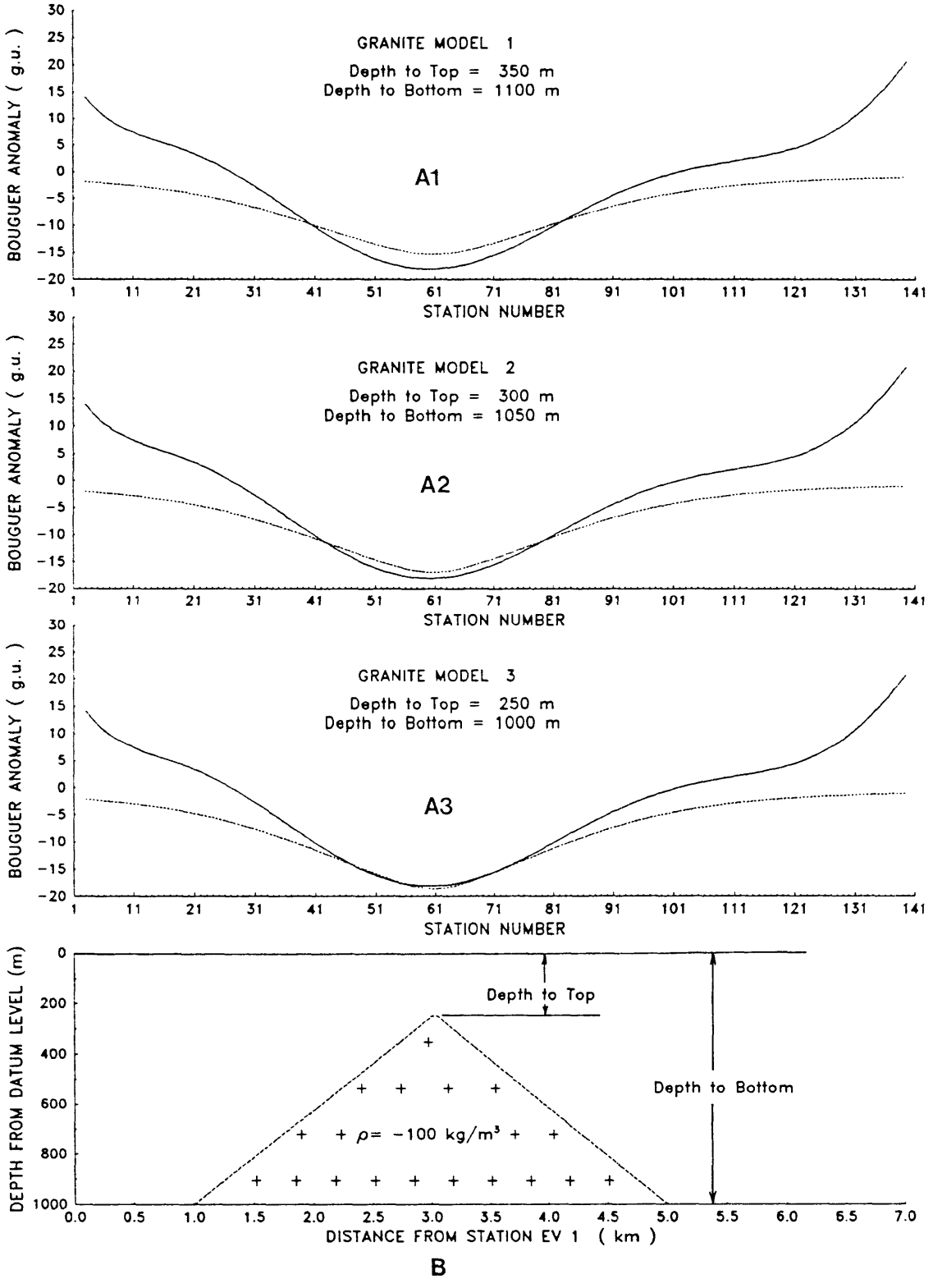

Figure 5.7 (A1-A3) The 7-km observed gravity profile (drawn as a solid line) and the computed gravity anomaly profiles (drawn as broken lines) generated by the granite models 1, 2 and 3 described in Section 5.2.2 and (B) Parameters and shape of the granite model

a point vertically above the causative structure (Al - Chalabi, 1971). For this reason it is inferred that the increase in observed gravity towards both sides of the profile is caused by other bodies that are denser than the Emmaville volcanics enclosing the granite. Geological maps show that the Tent Hill and Gulf Siltstone-Argillite Formations are exposed at the southern and northern part of the 7-km traverse line, respectively. Density measurements described in Section 3.3.1 on surface samples of these geologic formations generally revealed higher density values than those found for samples of the Emmaville volcanics. To approximate this geologic situation, bodies with positive density contrast relative to the Emmaville volcanics were added to the models as shown in Figures 5.8 and 5.9. This was sufficient to match the observed gravity profile with both the granite (Figure 5.8) and the basin model (Figure 5.9).

Arguments can be put forward against the basin model on the basis of topography and rock density. The topography along the profile demonstrates elevated areas (hills) just over the basinal structure as shown in Figure 5.8. Density measurements do not indicate the presence of systematically lower densities over the assumed basin formation relative to the Emmaville volcanics. Weathering could produce a low-density layer near the surface but it appears unlikely that the weathered layer has the trapezoidal shape indicated by gravity modelling and extends to depths of several hundred metres. Evidence from drillholes EZL-1 and EZL-2 located to the east of the profile shows that any weathered layer if present extends only to depths of the order of 20 m. This is not sufficient to explain the gravity data.

The granite model is more amenable to previously available geological information and the present density measurements. Although the existence of a granitic rise depicted in Figure 5.8 still has to be confirmed by drilling, arguments may be put forward in favor of the granite model as an interpretation of the anomaly:

1. the low frequency characteristic of the anomaly suggests that it is caused by a subsurface source;

2. both its length and magnitude indicate that the causative body is very broad, and

3. the model approximates Stegman's model described in Chapter 2.

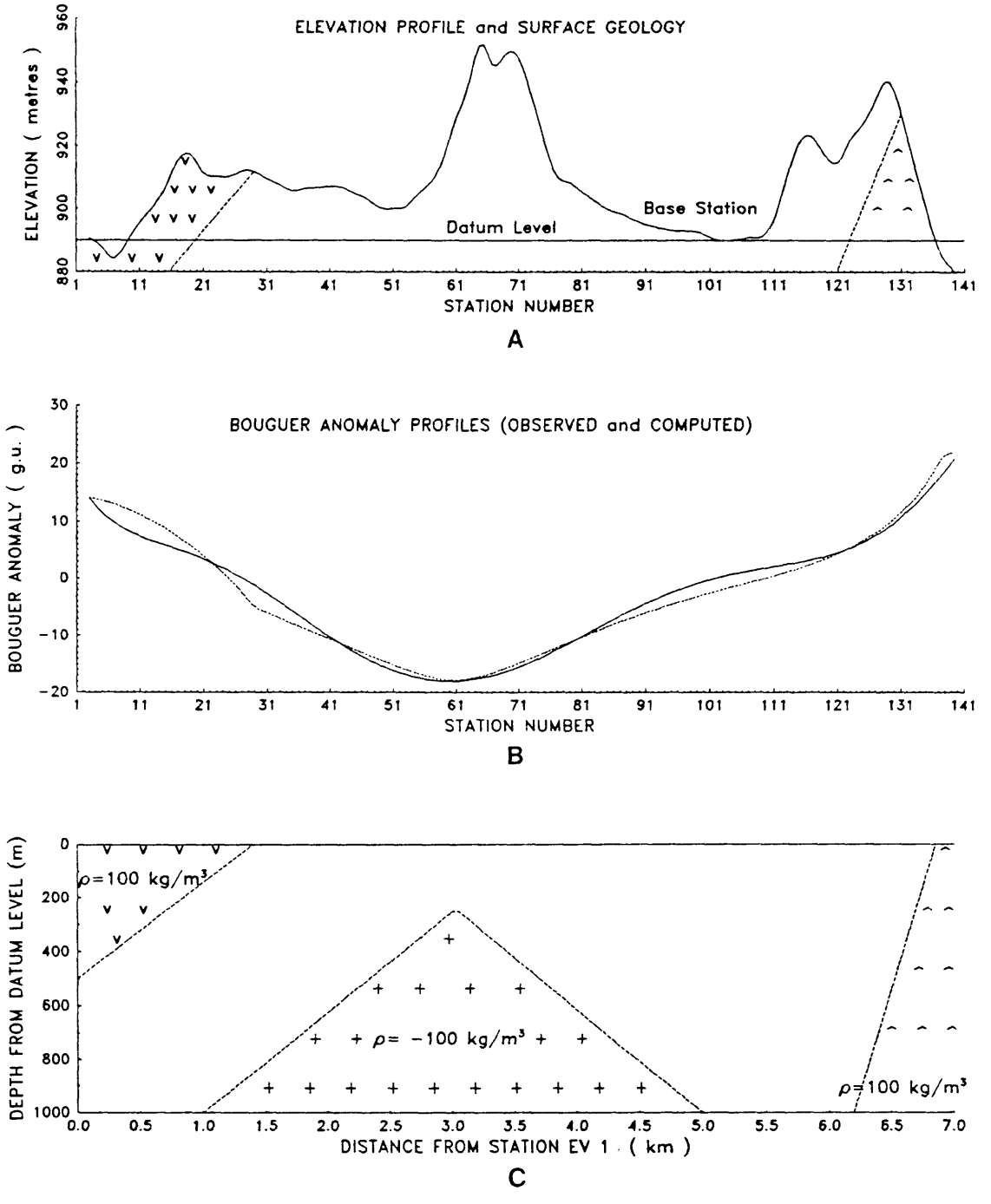

Figure 5.8 (A)The elevation profile and the surface geology (contact between formations were inferred from the surface evidence and ages of the formations), (B) The observed gravity profile (solid line) and the computed anomaly profile (broken line) generated by the geological model shown in (C) which consists of the granite model intruding into the Emmaville Volcanic Formation and the bounding Gulf Siltstone-Argillite and Tent Hill Volcanic Formations.

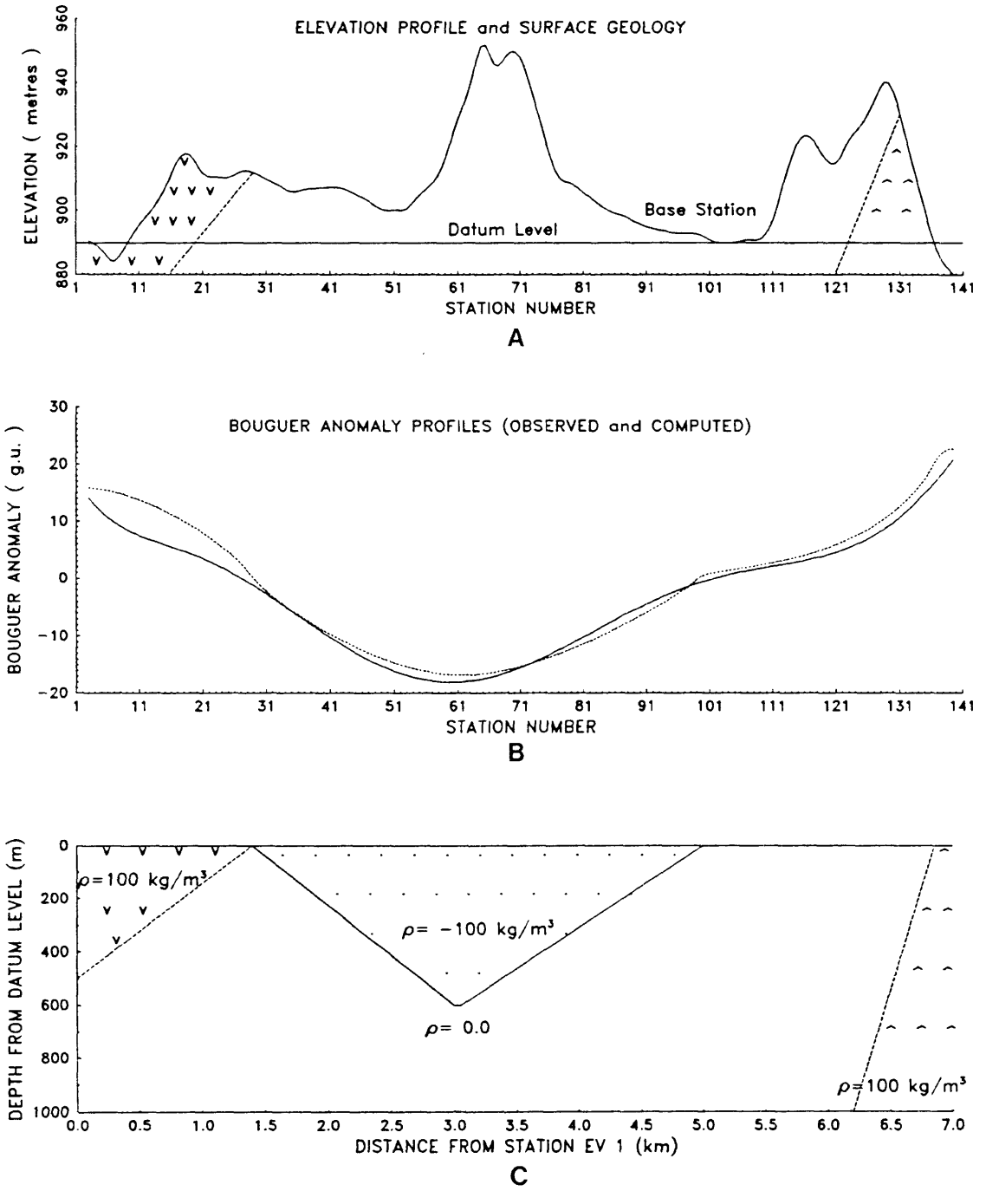

Figure 5.9 (A) The elevation profile and the surface geology which is exactly similar to Figure 5.8A, (B) The observed gravity profile (solid line) and the computed anomaly profile (broken line) generated by the geological model shown in (C) which consists of a basinal structure overlying the Emmaville Volcanic Formation and the bounding Gulf Siltstone-Argillite and Tent Hill Volcanic Formations.

Chapter 6

CONCLUSION AND RECOMMENDATION

The original objective of this study was to assess the potential of using the gravity method in detecting and delineating the granite cupola underlying the tin-bearing sediments near Emmaville, New South Wales. Models proposed for the genesis of tin-tungsten mineralization in the nearby Taronga mining area are associated with granite cupola structure. The density contrast between the low-density granite cupola and the overlying high-density metamorphosed sediments may give rise to gravity anomalies which, if detected, may define areas of future exploration activities.

One area chosen for a detailed gravity survey is located east of Emmaville where a 2 km x 2 km grid with a station spacing of 50 m was established. This area was chosen because it is known for the occurrence of tin mineralization from past mining activities. The resulting Bouguer gravity map is characterized by a broad minimum of 20 g.u. over the Emmaville Volcanic Formation relative to the neighbouring Tent Hill Volcanic and Gulf Siltstone-Argillite Formations. Small-scale minima on the gravity map are associated with minor intrusive bodies of granodiorite that outcrop in the area. These small-scale anomalies were attenuated to a large extent by upward continuation of the gravity field to 200 m above the datum level, indicating that they are caused by near-surface structures. A broad minimum became the dominant feature in the upward continuation map. One simple explanation is based on lateral variations of rock formations as indicated by the surface geological map. Density measurements on surface rock samples revealed slightly lower densities for the Emmaville volcanics relative to the adjacent formations. Assuming a density contrast of $100 kg/m^3$ results in a thickness of about 500 metres for the low-density Emmaville volcanics to account for a gravity anomaly of 20 g.u. Although this interpretation is consistent with surface geology, other factors such as a granite cupola may also produce the observed anomaly. To carry out a more detailed interpretation of the gravity anomaly additional data are required, such as sufficiently deep drillhole and/or seismic data that were not available during the course of this study. In addition, a more widely spaced grid should extend well outside the 2 km x 2 km area investigated in this study. This would allow gravity anomalies possibly related to the granitic cupola of the Mole Granite to be outlined more clearly than is possible with currently available data.

To assess the potential for such an extended grid survey, gravity readings were taken along a 7-km N-S traverse line. The Bouguer gravity anomaly along this line is characterized by a pronounced minimum of the order of 30 g.u. No indication was found for a systematic rise in the gravity anomaly from north to south (or away from the outcropping Mole Granite) which could have been indicative of the dipping top of the underlying Mole Granite and which is observed closer to its outcrop (Hutagaol, 1986).

The causative body responsible for the 7-km long-wavelength low-amplitude anomaly may either be a basinal structure filled with weathered Emmaville volcanics or a rise in the Mole Granite intruding into the Emmaville Volcanic Formation, which is in turn flanked by the Gulf Siltstone-Argillite Formation in the north and the Tent Hill Volcanic Formation at its southern boundary. The relatively small density contrast between the metamorphosed sediments of the Emmaville Volcanic Formation and the Mole Granite adds to the problem of identifying the causative body.

Although favouring the granite model because of its amenability to the geological evidence, the writer believes that further studies and investigations using other geophysical methods and/or the more direct and reliable drilling need to be done before any attempt can be made to establish a model for tin mineralization in the area.

The application of the gravity method as an exploration tool in finding granite cupolas or apices underlain by metamorphosed sediments in the New England tin belt is obviously accompanied by difficulties. The most important of these is the problem of finding a unique solution to the anomaly (of relatively smaller magnitude) on the basis of the gravity and surface geological data only. Further surveys and studies are therefore necessary to confirm the interpretations proposed in this thesis. The use of other geophysical techniques not affected by the ambiguities normally inherent in gravity surveys is recommended to establish the existence and features of the proposed buried granite cupola in the studied area. If a good impedance contrast exists between the Emmaville volcanics and the presumed granitic intrusion, then the seismic method is probably best suited to achieve the objectives of determining the depth to, and the shape and features of the proposed granite cupola.